Article

Experimental Investigation and CFD Simulation of Cryogenic Condenser

Seyedsajjad Jazayeri [1], Afham Pourahmad [2], Seyyed Amirreza Abdollahi [3], Amin. Hassanvand [4], Falah Alobaid [5] and Babak Aghel [5,6,*]

1 Department of Chemical Engineering, Azad Abadan University (Abadan Azad University), Abadan 1477893855, Iran; sajjad.jazayeri64@yahoo.com
2 Department of Polymer Engineering, Amirkabir University of Technology (Tehran Polytechnic), Tehran 1591634311, Iran; pourahmad_a@aut.ac.ir
3 Faculty of Mechanical Engineering, University of Tabriz, Tabriz 51368, Iran; s.a_abdollahi@yahoo.com
4 Department of Polymer Engineering, Faculty of Engineering, Lorestan University, Khorramabad 44316-68151, Iran; amin.hassanvand@gmail.com
5 Institut Energiesysteme und Energietechnik, Technische Universität Darmstadt, Otto-Berndt-Straße 2, 64287 Darmstadt, Germany; falah.alobaid@tu-darmstadt.de
6 Department of Chemical Engineering, Faculty of Energy, Kermanshah University of Technology, Kermanshah 6715685420, Iran
* Correspondence: babak.aghel@est.tu-darmstadt.de; Tel.: +49-(61)-511622673; Fax: +49-(06)-1511622690

Abstract: In this research, experimental investigation and the computational fluid dynamic (CFD) simulation of a cryogenic condenser for oxygen liquefaction was carried out. The liquid nitrogen was used as a cooling fluid. In the simulation section, a three-dimensional model with a structured mesh with high mesh quality for aspect ratio and skewness was considered. The multi-phase flow inside the condenser was studied numerically, using the volume of fluid (VOF) method. This work also examined the assessment of the vapor generation rate during the condensation of oxygen, based on the boiling heat transfer mechanism and the unique physical characteristics. The experiment was conducted to examine the simulation results. The effect of liquid nitrogen height on the oxygen mass flows was investigated using computational fluid dynamics (CFD). The average deviation of the CFD predictions from the available experimental oxygen mass flows was 17%.

Keywords: computational fluid dynamic; cryogenic condensation; boiling; volume of fluid

1. Introduction

Heat exchangers are becoming increasingly important in various industries and systems. They are used in a wide range of applications, including food production, power generation, petrochemicals, and biomedical instruments. Heat exchangers are also widely used in cooling and heating systems to create specific temperature environments for humans [1–4]. Since the efficiency of heat exchangers is crucial for cost reduction, engineers and researchers have focused on improving these devices and have developed various types of heat exchangers for different applications. Shell-and-tube heat exchangers and double-pipe heat exchangers are the most commonly used types of heat exchangers, and are widely applied in different industries. These two types of heat exchangers are designed to meet different requirements for specific applications and working conditions. Overall, the importance of heat exchangers in various industries and systems has led to significant research and development efforts to improve their efficiency and performance. The availability of different types of heat exchangers allows for customization for specific applications and working conditions, resulting in cost-effective solutions for heat transfer [5–8].

The cryogenic-based separation using the distillation column has recently attracted researchers' attention in a wide range of industrial applications. Condensers are likely the

most important side apparatus utilized to increase the heat transfer in this cryogenic-based separation [9,10]. Among the different heat sources, conductive heat plays a significant role in vapor generation during the initial step of the spill [11,12]. Previous research suggests several successive regimes for the conductive heat transfer during a cryogenic liquid spill, i.e., nucleate, transition, and film boiling [13–16]. These successive boiling regimes are schematically shown in Figure 1.
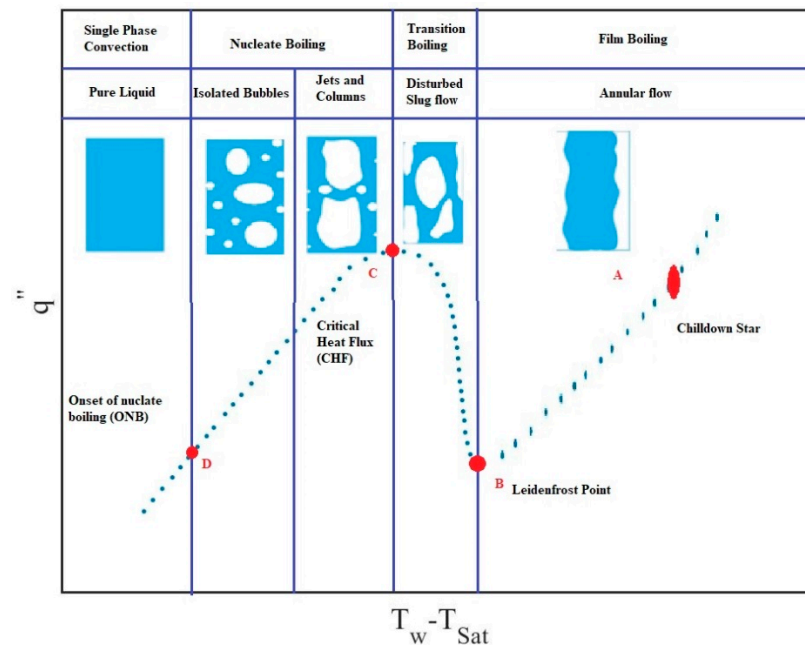
Figure 1. The reported successive boiling regimes for the cryogenic liquid spill (q'' is heat flux [kW/m^2] and T_w-T_{sat} is deference temperature [K]) [17].

As shown in this graph, before location A (known as the starting point of the nucleate boiling), where the surface temperature must be under saturation, we have no bubbles and there is a free convection area. According to the schematic diagram, the liquid begins to boil with isolated bubbles as the temperature is raised. This region is called nucleate boiling. In the A to B region, some isolated bubbles are created at the nucleation spots and detached from the hot surface. Increasing the temperature increases the number of nucleation active sites, generated bubbles, and bubbles' collision and coalescence. The section corresponding to points B to C is termed transition boiling, i.e., unstable film boiling. Point B (the Leidenfrost point) presents the minimum amount for the heat flux, and vapor completely covers the hot surface. Finally, completely covering the substrate surface with bubbles creates a continuous film between the solid and liquid, decreasing the heat flux rate (points C to D in the curve). The conduction and radiation inside the vapor phase are responsible for the transfer of heat between the hot surface and the liquid phase. The variation in the heat flux for the liquid nitrogen (N_2) boiling as a function of temperature is similar to that in Figure 1.

The saturated temperatures of oxygen and nitrogen in 1 atm are 91 and 77 K, respectively, so we can consider the temperature of the wall equal to 84 K (the mean temperature). The temperature difference between the wall and the saturated temperature of nitrogen is 13 K, so, according to Figure 1, we are in the nucleation boiling regime.

Over the years, there have been several experimental studies conducted on the boiling behavior of nitrogen in channels. One such study by Klimenko and Sudarchikov [18] investigated the boiling behavior of nitrogen in a vertical pipe. The authors analyzed the effect of pressure, mass flow, and heat flux on the overall heat transfer coefficient. This involved measuring the temperature, pressure, and flow rate of nitrogen and studying their impact on the heat transfer rate.

Another study by Ishimoto et al. [19] used the unsteady thermal non-equilibrium two-fluid approach to investigate the thermodynamic impact on the bubble flow behavior of liquid nitrogen in a horizontal rectangular nozzle. This involved modeling the behavior of the liquid and vapor phases separately, and analyzing the thermal non-equilibrium between them. The authors used numerical simulations to investigate the behavior of nitrogen boiling under different conditions in the horizontal rectangular nozzle.

Li et al. used the two-fluid model for simulating the boiling behavior of liquid nitrogen inside a vertical cylindrical tube [20]. An empirical correlation is also incorporated into the simulation stage for estimating water properties. Cryogenic fluids have large compressibility and small latent heat of vaporization compared to ordinary liquids.

These studies provide valuable insights into how different parameters affect the heat transfer rate and bubble flow behavior of nitrogen boiling in channels. Such information is crucial for optimizing the design and operation of cryogenic systems that use nitrogen as a coolant, such as in the liquefaction of gases or in superconducting applications.

Several works have been carried out on condensers, experimentally. Zhang et al. [21] experimentally investigated the heat transfer in a condenser with a liquid–vapor separator to measure the separation ratio and its effect on heat transfer. The experiments used a separator attached to a condenser that could measure the separation ratio to compare the heat transfer rates with and without the liquid–vapor separator. The results showed the limitations of the liquid–vapor separator and how the liquid–vapor separator separation ratio varies for various vapor mass velocities and mass flow rates for cooling water. Zhang et al. [22] used a numerical and experimental study to evaluate the performance of a power plant condenser. Peng and Jia [23] presented a condenser design method based on the effect of the vapor mass flow rate and the vapor fraction on the heat transfer and pressure drop. Their studies indicated the potential for improving heat transfer by using a liquid–vapor separator to remove the condensate. Oh, et al. [24] and Won [25] experimentally verified the improved performance of the liquid–vapor separation condenser. Some experimental studies [26–28] have reported that flow maldistributions are very likely in the headers with two-phase refrigerants.

Tu [29] and Yeoh [30] made a correct prediction of subcooled boiling in the relationships between the size of distributed bubbles and the area of concentration and between the partition of the wall heat flux and the bubbles' diameter. They also stated that the bubble frequency is also another important factor for predicting the true behavior of the subcooled boiling. Zuber [31] studied and modeled a film boiling on a horizontal surface and concluded that an inconsistency exists between the developed model and the Rayleigh−Taylor hydrodynamic concept. Therefore, Zuber suggested bounding for the nearest distance of evolving bubbles by Taylor's "critical" and "most dangerous" wavelengths [31]. In addition to this conclusion, by considering the distance between the bubbles, a square cell could be formed by two bubbles evolving per cycle, and he consequently assumed the Leidenfrost point.

Chen et al. [32] studied liquid–vapor-separated condensers with three tube pass arrangements and evaluated their ability to automatically separate the liquid and vapor during the condensation in a split-type air conditioner. They [33] also presented an algorithm to predict the in-channel thermodynamic performance of the liquid–vapor-separated condenser.

CFD is an applicable tool for modeling the multiphase flow, and was reported in several research works [34–36]. Son and Dhir [37] used numerical simulations to investigate the heat transfer that occurs during pool boiling. Pool boiling is a type of boiling that occurs when a liquid is in contact with a heated surface, such as a pot of water on a stove. Dhir's simulations provided a detailed analysis of the heat transfer process, including the formation and growth of bubbles on the heated surface and the transport of heat from the surface to the bulk fluid. The study used a combination of theoretical models and numerical simulations to analyze the heat transfer process in detail. The results of the study provided valuable insights into the underlying physics of pool boiling, and can be used to

optimize the design and operation of heat transfer systems in various applications, such as power generation and refrigeration.

They introduced a hybrid scheme with the capability of studying both nucleate and film boiling [38]. In this study, Son and Dhir used a numerical simulation technique called the level-set method to investigate film boiling near critical pressure. Film boiling is a type of boiling that occurs when a superheated surface is in contact with a liquid. The level-set method is a numerical technique that can accurately simulate the motion of interfaces between fluids. The authors simulated the behavior of a liquid–vapor interface near a superheated surface and analyzed the heat transfer characteristics, including the heat transfer coefficient and the critical heat flux. The study provided a detailed analysis of the fluid dynamics and heat transfer mechanisms that occur during film boiling near critical pressure. The results of the study can be used to optimize the design and operation of heat transfer systems in various industrial applications, such as nuclear power generation and rocket propulsion. Moreover, to gain a better understanding of a pattern for steady-state bubble release, they considered near-critical conditions for water at the axisymmetric horizontal film boiling [39]. Panzarella et al. [40] performed a nonlinear evolution equation and provided the modeling for water film boiling for which lubrication approximation was used. In another study, Banerjee [39] simulated a subcooled system containing water film boiling on a horizontal disk. Juric [41] added interfacial source terms to the continuity equations to simulate the horizontal film boiling for low- to high-density fluids. This modification removed the iterative stage and improved the prediction accuracy of Esmaeeli et al. [42,43]. Welch [44] utilized the VOF scenario to simulate the saturated horizontal film boiling with the heat transfer conjugation. In a further study, Welch and Rachidi [45] applied the aforementioned method to the simulation of film boiling of water at the interface of steel. To study the effect of shape, Yuan et al. [46] performed simulations for the water film boiling around a sphere with a nonorthogonal body-fitted coordinate. Agarwal and coworkers employed a variant of the VOF method to analyze the transient bubble release patterns and transport coefficients of the water film boiling at T = 100 K and P = 2.19×10^7 Pa [47]. They also monitored the influence of fluid properties. The hybrid method including level-set and volume of fluid (CLSVOF) has been used by Tomar et al. [48,49] and Hens et al. [50] to study the water and R134a refrigerant close and far away from the critical pressure. In another similar work, Welch and Biswas [51] and Tomar et al. [52] simulated the impact of electrical potential on the heat transfer of film boiling. Moreover, Liu et al. [17] investigated the pool boiling of liquid nitrogen using ANSYS Fluent. In this study, Liu et al. used computational fluid dynamics (CFD) simulations to model the pool boiling behavior of a cryogenic liquid. Pool boiling is a type of boiling that occurs when a liquid is in contact with a heated surface. Cryogenic liquids, which are liquids that are kept at extremely low temperatures, are commonly used in a variety of industrial applications, including cooling systems for electronics and in the liquefaction of gases. The authors developed a CFD model to simulate the pool boiling behavior of a cryogenic liquid and analyzed the heat transfer mechanisms that occurred during the process. The study provides valuable insights into the behavior of cryogenic liquids during pool boiling, which is important for optimizing the design and operation of cryogenic cooling systems. The results of the study can be used to improve the efficiency and safety of cryogenic cooling systems in various industrial applications.

From the above-mentioned studies, several researchers have studied film boiling by computational scenarios, bubble formation dynamics, corresponding heat transfer behavior, and simulation of horizontal film boiling. However, there are not any noteworthy attempts to simulate the cryogenic fluid boiling and condensation process coupled together or even simultaneously in a vertical tube.

In this study, an experimental study and the CFD approach were used to investigate an air separation cryogenic condenser. This research studies cryogenic condenser heat transfer and its behavior in diverse operational situations. The multi-phase flow inside the condenser was studied numerically, using the VOF method. Simulation results were

compared with experimental data. The simulation results were in good agreement with the experimental data. In addition, cryogenic condensers were simulated at different liquid nitrogen heights to find the equation rate of nitrogen evaporation and oxygen condensation.

2. Simulation Stage

2.1. Main Equations

In this work, the VOF model is applied to compute multiphase flows in the interface of the gas–liquid. In this study, the CFX-18 was used for simulation. The VOF technique is suitable for monitoring the interface between two separated phases such as gas and liquid [53–55]. In this technique, the parameters such as velocity and pressure are linked to both the vapor and liquid phases, and correspond to volume-averaged characteristics [56,57]. The continuity equation for the volume fraction of the vapor phase has the following form [58–61]:

$$\frac{\partial}{\partial t}(\alpha_v \rho_v) + \nabla \cdot \left(\alpha_v \rho_v \vec{v}\right) = S_m \tag{1}$$

where the mass source S_m is defined in Equation (7). The volume fraction of the liquid is calculated on the following constraint [62]:

$$\alpha_l + \alpha_v = 1 \tag{2}$$

Liquid and vapor have a shared velocity field in the fluid domain. The velocity field is obtained by solving the momentum equation:

$$\frac{\partial}{\partial t}\left(\rho \vec{v}\right) + \nabla \cdot \left(\rho \vec{v} \vec{v}\right) = -\nabla p + \nabla \cdot \mu\left(\nabla \vec{v} + \nabla \vec{v}^T\right) + \rho \vec{g} + \vec{F} \tag{3}$$

The effect of surface tension is modeled using the continuum surface force (CSF) model. The surface tension force is added to the momentum equation as a source term, which is the F in Equation (3).

$$F = \sigma \frac{(\alpha_v \rho_v \kappa_l \nabla \alpha_l + \alpha_v \rho_v \kappa_v \nabla \alpha_v)}{0.5(\rho_v + \rho_l)} \tag{4}$$

where σ is the surface tension coefficient. κ is the curvature given by

$$\kappa = -\nabla \cdot \left(\frac{\nabla \alpha}{|\nabla \alpha|}\right) \tag{5}$$

Similar to the momentum equation, a single energy equation is solved throughout the domain:

$$\frac{\partial}{\partial t}(\rho E) + \nabla \cdot \left(\vec{v}(\rho E + p)\right) = \nabla \cdot (k \nabla T) \tag{6}$$

Mass and heat transfer rates can be defined by the Lee model [62] to simulate the phase change process. The mass transfer source shown on the right side of Equation (1) can be described as follows:

$$S_m = \dot{m}_{lv} - \dot{m}_{vl} \tag{7}$$

If $T_l > T_{sat}$ (evaporation),

$$\dot{m}_{lv} = \beta_l \alpha_l \rho_l \frac{(T_l - T_{sat})}{T_{sat}} \tag{8}$$

If $T_v < T_{sat}$ (condensation),

$$\dot{m}_{vl} = \beta_v \alpha_v \rho_v \frac{(T_{sat} - T_l)}{T_{sat}} \tag{9}$$

where $\dot{m}_{lv}$ and $\dot{m}_{vl}$ are evaporation and condensation mass transfer rates, respectively. Mass transfer rates have positive values when mass transfers from liquid to vapor. β_l and β_v are the evaporation and condensation coefficients, respectively.

2.2. Numerical Procedure

The schematic of the applied domain is shown in Figure 2a. Outlet boundary conditions have been imposed on the top of the nitrogen domain and opening boundary conditions have been considered for the bottom of the oxygen domain.
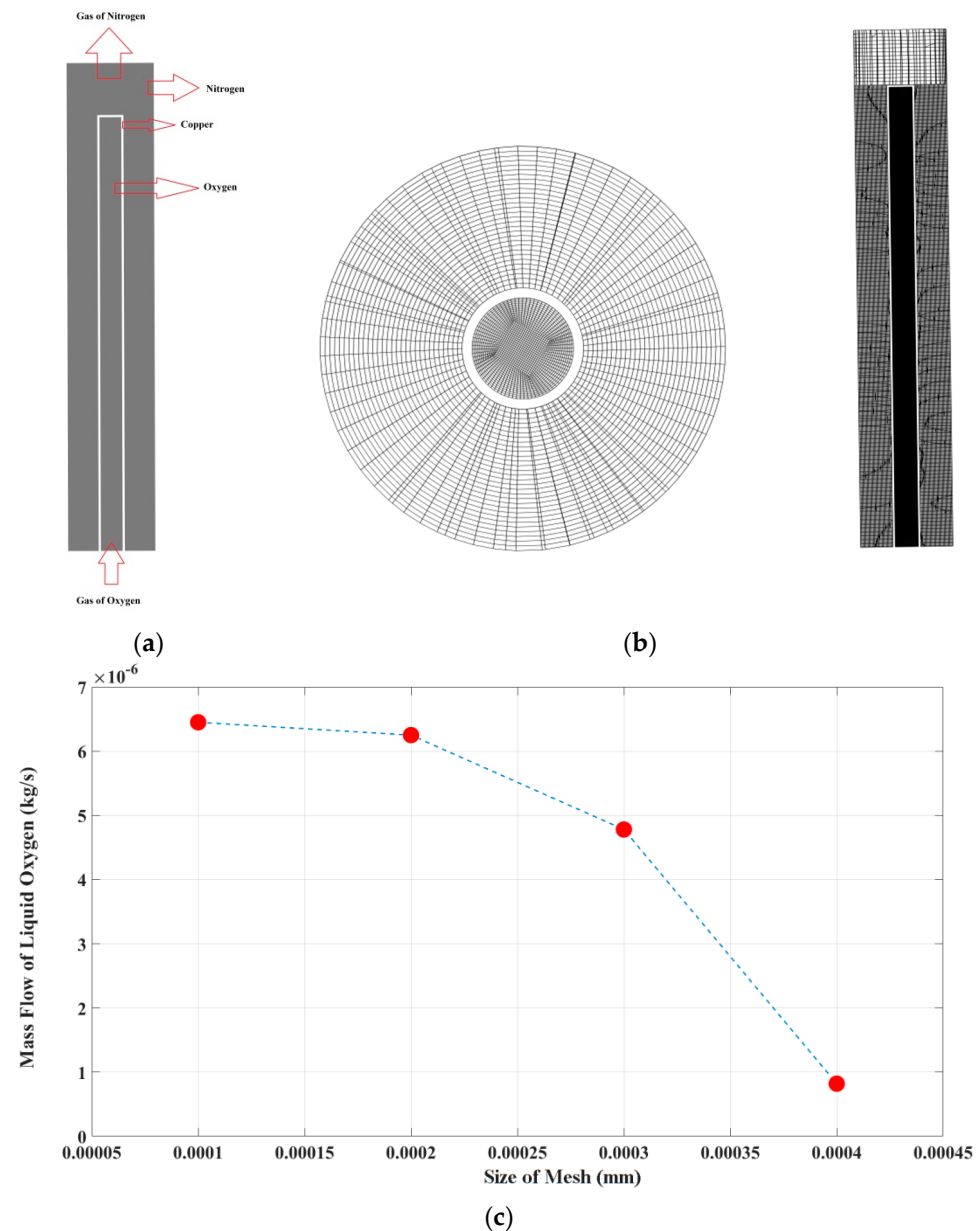
Figure 2. Numerical setup and validation of the current study. (**a**) Computational domain and boundary conditions. (**b**) Generating grid. (**c**) Mesh independence test.

The liquid nitrogen is located inside the nitrogen section and around the copper tube. The oxygen vapor enters from the end of the tube and begins to condensate when it moves along the tube and turns into a liquid, and it is removed from the end of the tube. Liquid nitrogen starts to boil due to the heat, and nitrogen vapor exits above the nitrogen chamber. The physical characteristics of the fluids are displayed in Table 1.

Table 1. Characteristics of fluids [63].

Fluid	ρ $(\mathbf{kg/m^3})$	$\mu(\mathbf{cP})$
Nitrogen-Gas	1.138	0.01663
Oxygen-Gas	1.299	0.01919
Nitrogen-Liquid	806.08	1.6065
Oxygen-Liquid	1142	1.19582

It is necessary to analyze the effect of mesh size on the accuracy of the numerical results before the model validity checking. Hypercube-shaped meshes were used for the whole pipe domain, and tetrahedral-shaped elements were generated in the tube center. Initially, elements with average side lengths of 0.0004, 0.0003, 0.0002, and 0.0001 m were used to establish the computational domain. Upon solving the flow field, volume fraction, and energy equations, the corresponding mass flow of liquid oxygen was calculated. Four different meshes with sizes ranging from 0.0001 to 0.0004 m were examined in this regard (See Figure 2c). This figure confirms that the difference between the 0.0002 and 0.0001 m mesh sizes under the operating conditions is less than 1%. Therefore, it can be claimed that the fine mesh size is sufficient enough for reaching grid-independent solutions. For the trade-off between the accuracy and computational cost, a model with 0.2 mm elements was used in this study (Figure 2b). To ensure the mesh quality, the histogram for the parameter's aspect ratio and skewness were plotted. As the aspect ratio of most elements did not exceed 3, and skewness was also within the very reasonable range of less than 0.5, it was concluded that the mesh quality was fully acceptable.

2.3. Experimental Setup

The heat exchanger used in this research is made of 50 high-purity copper tubes, 0.2 m in height, with an outer diameter of 0.2 m and a thickness of 0.001 m. The pipes are welded from the bottom of the plate. Liquid nitrogen is placed around the tubes and gaseous oxygen is placed inside the tubes. Due to the temperature difference between liquid nitrogen and liquid oxygen, liquid nitrogen causes gas oxygen to be collected in liquid form. A type K thermocouple (3–1533 K, 0.4% accuracy) was used to measure the temperature. In addition, a Wika S-10 pressure gauge (0–10^6 Pa absolute pressure, 0.5% accuracy) was used to measure pressure and pressure drop. The operation of the refrigeration condenser is as follows: first, liquid nitrogen enters the condenser shell. Due to the large temperature difference between the shell and the liquid nitrogen, it takes about two hours for the nitrogen to reach equilibrium and the temperature in the tank to become the same as in the shell. At this time, the liquid nitrogen evaporates and the shell temperature drops. After the temperature reaches steady-state in the shell, we introduce oxygen gas from the bottom and inside the tubes using a mass flow controller (BROOKS Instrument, 0–0.005 m^3/S, ±0.6% accuracy). Oxygen gas is exchanged through the cold copper pipes, and turns into liquid oxygen. Due to the conversion of gaseous oxygen into liquid, the pressure on the side of the liquid oxygen slowly decreases, and liquid oxygen must be injected into the system to keep the pressure constant at atmospheric pressure. The amount of liquid oxygen produced can be obtained in two ways: either by measuring the amount of oxygen injected into the system based on time, or by measuring the amount of liquid oxygen produced and calculating the oxygen liquefaction rate. The experimental tests were performed for the entire heat exchanger, and the results were analyzed to better understand the behavior of the system. Figure 3 shows the copper pipes and the schematic of the heat exchanger.

(A)   **(B)**
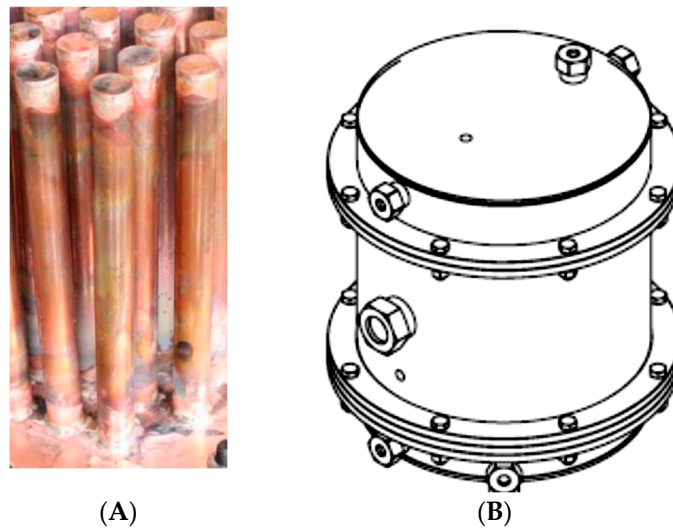
Figure 3. (**A**) Copper pipes (**B**) The schematic of the heat exchanger.

3. Results and Discussion

Figure 4 shows the liquid volume of oxygen within the tube of the condenser. The results indicate that the liquid volume of oxygen is higher near the bottom of the tube compared to the middle of the tube. This is because the liquid nitrogen used to cool the condenser is added from the top, causing the temperature gradient to be highest near the top of the tube. As a result of this temperature gradient, the oxygen gas begins to condense from the top of the tube and the thickness of the liquid oxygen layer increases as it moves down the tube. This is because the colder temperature near the top of the tube causes the oxygen to condense into liquid, which then flows down the tube, due to gravity. As the liquid oxygen flows down the tube, it accumulates, and the volume of liquid oxygen increases towards the bottom of the tube.
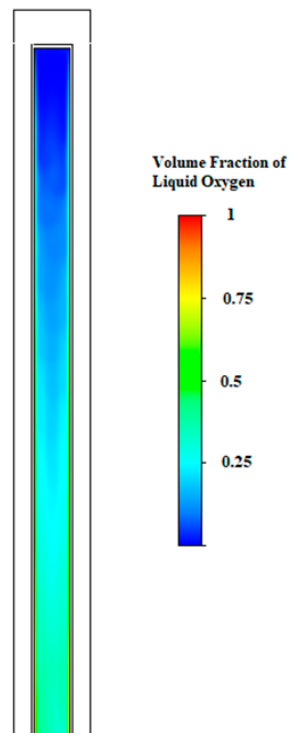
Figure 4. The contour of the volume fraction of liquid oxygen.

The liquid volume of oxygen is also affected by the level of liquid nitrogen in the condenser. The liquid volume of oxygen at the bottom of the tube is higher because the liquid nitrogen level is higher at the bottom, which creates a greater pressure difference between the top and bottom of the tube. This pressure difference helps drive the flow of liquid oxygen toward the bottom of the tube.

Figure 5 shows the evaporation rate of liquid nitrogen and the production of liquid oxygen for different heights of nitrogen, as measured experimentally and predicted by numerical simulation. The results indicate that the mass flow rate of liquid oxygen at the outlet is highest at a nitrogen height of 0.2 m and is approximately 3.5 L/h in the 3D model. The corresponding mass flow rate of vapor nitrogen at the outlet is 3.86 L/h.
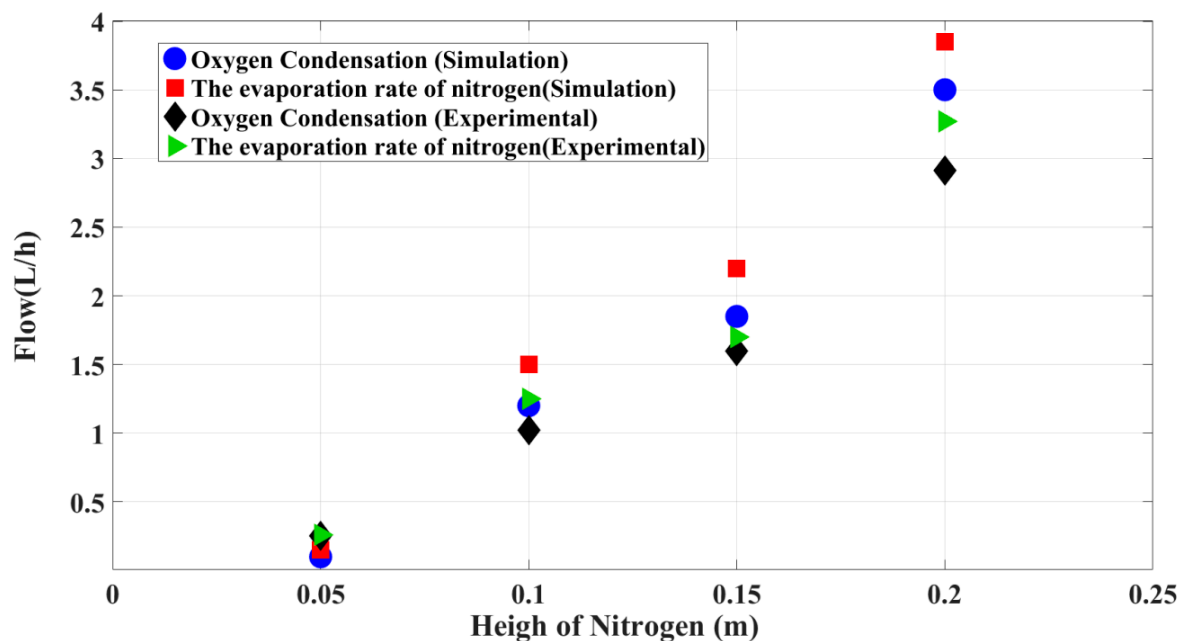
Figure 5. The experimental and numerical evaporation rate of liquid nitrogen and the production of liquid oxygen for different heights of nitrogen.

The experimental results show that the rate of nitrogen evaporation is about 3.3 L/h when the nitrogen height is 0.2 m. This suggests that the numerical simulation can predict the behavior of the system with reasonable accuracy, given that the experimental and simulation results are in good agreement. The average relative error between the experimental data and numerical simulation is 17%, indicating that the simulation predictions are within acceptable limits of accuracy.

In similar works, the authors compared the numerical results with experimental data to validate the accuracy of the model. In the research work presented by Dhir [48], the numerical simulations were found to be in good agreement with experimental data for the heat flux and bubble dynamics. However, there were some discrepancies between the numerical results and experimental data for the bubble departure diameter and frequency. The author discusses possible reasons for these discrepancies, such as uncertainties in the experimental measurements and simplifications in the numerical model.

In another work, numerical simulations were found to be in good agreement with experimental data for the void fraction and pressure drop under both static and rolling motion conditions. However, there were some differences between the numerical results and experimental data for the local void fraction distribution and the boiling heat transfer coefficient. The authors discussed possible reasons for these discrepancies, such as uncertainties in the experimental measurements and simplifications in the numerical model.

The results of this study provide valuable insights into the behavior of a cryogenic condenser, and can be used to optimize the design and performance of such systems. For

instance, the finding that the highest mass flow rate of liquid oxygen occurs at a nitrogen height of 0.2 m can inform the design of the condenser, to ensure that the liquid nitrogen is added at the optimal height for maximum production of liquid oxygen. Additionally, the knowledge that the rate of nitrogen evaporation is about 3.3 L/h at this height can inform the operational parameters of the system, such as the flow rate of the liquid nitrogen, to ensure that the production of liquid oxygen is optimized.

Figure 6 shows the temperature of the oxygen vapor along the length of the pipe. The results of the study indicate that the maximum temperature is found near the inlet of the pipe, which is expected because the vapor is entering the pipe at a higher temperature. The maximum temperature observed is around 90 K, which is the oxygen saturation temperature at a pressure of 1 atm. This means that the oxygen vapor is close to its boiling point and is likely to condense as it moves along the pipe.
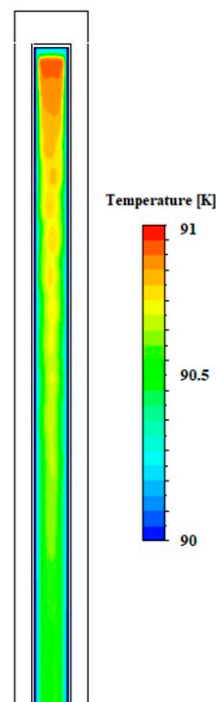
Figure 6. The temperature of oxygen vapor.

The lowest temperature is observed on the walls of the pipe, which is expected because the walls are in contact with the cooling medium and are therefore colder than the vapor. This temperature gradient between the vapor and the walls of the pipe is important because it influences the rate of condensation of the oxygen vapor. As the vapor moves along the pipe and comes into contact with the colder walls, it loses heat and begins to condense into liquid oxygen. The rate of condensation is influenced by various factors such as the temperature gradient, pressure, and flow rate of the vapor.

Figure 7 shows the velocity contour of the oxygen vapor. The results suggest that the natural motion of the vapor within the pipe is accurately captured by the simulations. This is an important finding, because it indicates that the numerical model used in the simulations is capable of capturing the complex flow behavior of the oxygen vapor as it moves along the pipe.

The behavior of the oxygen vapor in a cryogenic condenser is complex, and depends on various factors such as pressure, temperature, and flow rate. The accurate modeling of the flow behavior of the oxygen vapor is essential for the optimization of the design and performance of the cryogenic condenser. The findings of this study provide valuable insights into the behavior of oxygen vapor in a cryogenic condenser, and can be used to optimize the design and performance of such systems.
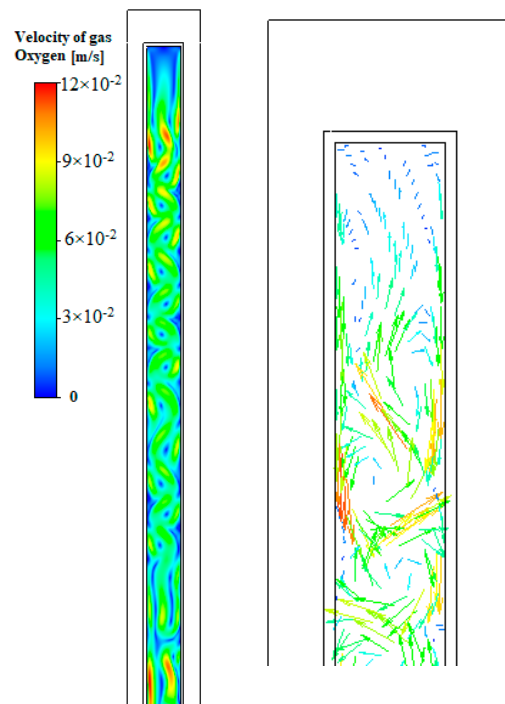
Figure 7. Oxygen steam velocity.

4. Conclusions

In this study, we investigated the performance of a cryogenic condenser using both experimental measurements and CFD simulations. Our analysis focused on the heat transfer characteristic of the condenser under various operating conditions, in addition to the reliability of the VOF to simulate the boiling behavior of liquid nitrogen using vertical geometry. The effect of nitrogen height was comprehensively investigated using the CFD. The obtained results show that the rate of liquid oxygen mass flow on the outlet is 3.5 [L/h] for the simulation at 200 mm nitrogen height. The corresponding mass flow of vapor nitrogen on the outlet is 3.86 [L/h]. Experimental results show that the rate of nitrogen evaporation is about 3.3 [L/h] with 20 cm high nitrogen. These results were in good agreement with the results obtained from the CFD simulations, which had an average relative error of 17% compared to the experimental data. Overall, our study provides a better understanding of the performance of cryogenic condensers and highlights the importance of using a combination of experimental and numerical methods to analyze complex thermal systems. The results of this study can be used to optimize the design and operation of cryogenic condensers for various applications in the chemical, pharmaceutical, and energy industries.

Conflicts of Interest: The authors declare no conflict of interest.

Nomenclatures

Latin symbols

E	energy	[J]
F	surface tension	[N/m]
g	standard gravity	[ms^{-2}]
h	enthalpy, heat transfer coefficient	[kJ·kg^{-1}], [kJ·m^{-2} K^{-1})]
k	conductive coefficient	[kg·m·s^{-3}·K^{-1}]
m	mass	[kg]
$\dot{m}$	mass transfer rate	[kg·m^{-3}·s^{-1}]
P	pressure	[Pa]
Q	heat transfer	[kJ]
S	mass source term	[kg·m^{-3}·s^{-1}]
T	temperature	[K]
t	time	[s]
v	velocity	[ms^{-1}]
V	volume	[m^3]
x,y,z	Cartesian coordinates	[m]

Greek symbols

α	volume fraction	[-]
β	coefficient	
ρ	density	[kg·m^{-3}]
κ	curvature	[-]
σ	stress	[kg·m^{-1}·s^{-2}]
∇	gradient	[-]
μ	viscosity	[kg·m^{-1}·s^{-1}]

Subscripts and indices

sub	subcooling temperatures
sat	saturation temperatures
m	mass
l	liquid
g	gas
vl	vapor–liquid

References

1. Xiang, J.; Yang, W.; Liao, H.; Li, P.; Chen, Z.; Huang, J. Design and thermal performance of thermal diode based on the asymmetric flow resistance in vapor channel. *Int. J. Therm. Sci.* **2023**, *191*, 108345. [CrossRef]
2. Ghazanfari, V.; Imani, M.; Shadman, M.M.; Amini, Y.; Zahakifar, F. Numerical study on the thermal performance of the shell and tube heat exchanger using twisted tubes and Al$_2$O$_3$ nanoparticles. *Prog. Nucl. Energy* **2023**, *155*, 104526. [CrossRef]
3. Jianhua, X.; Liangming, D.; Zhou, C.; Zhao, H.; Huang, J.; Sulian, T. Heat Transfer Performance and Structural Optimization of a Novel Micro-channel Heat Sink. *Chin. J. Mech. Eng.* **2022**, *35*, 38.
4. Liu, F.; Sun, Z.; Bian, H.; Ding, M.; Meng, X. Identification and classification of the flow pattern of hydrogen-air-steam mixture gas under steam condensation. *Int. J. Therm. Sci.* **2023**, *183*, 107854. [CrossRef]
5. Selimefendigil, F.; Öztop, H.F. Effect of a rotating cylinder in forced convection of ferrofluid over a backward facing step. *Int. J. Heat Mass Transf.* **2014**, *71*, 142–148. [CrossRef]
6. Yang, M.; Li, C.; Luo, L.; Li, R.; Long, Y. Predictive model of convective heat transfer coefficient in bone micro-grinding using nanofluid aerosol cooling. *Int. Commun. Heat Mass Transf.* **2021**, *125*, 105317. [CrossRef]
7. Yang, M.; Li, C.; Zhang, Y.; Wang, Y.; Li, B.; Jia, D.; Hou, Y.; Li, R. Research on microscale skull grinding temperature field under different cooling conditions. *Appl. Therm. Eng.* **2017**, *126*, 525–537. [CrossRef]
8. Wang, Y.; Zhai, W.; Zhang, H.; Cheng, S.; Li, J. Injectable polyzwitterionic lubricant for complete prevention of cardiac adhesion. *Macromol. Biosci.* **2023**, *23*, 2200554. [CrossRef]
9. Cao, Y.; Dhahad, H.; Khandakar, A.; Chowdury, M.; Ayari, M.; Alizadeh, S.; Vaferi, B. Employing computational fluid dynamics technique for analyzing the PACK-1300XY with methanol and isopropanol mixture. *Sci. Rep.* **2022**, *12*, 6588. [CrossRef]
10. Si, Z.; Yang, M.; Yu, Y.; Ding, T. Photovoltaic power forecast based on satellite images considering effects of solar position. *Appl. Energy* **2021**, *302*, 117514. [CrossRef]
11. Véchot, L.; Olewski, T.; Osorio, C.; Basha, O.; Liu, Y.; Mannan, S. Laboratory scale analysis of the influence of different heat transfer mechanisms on liquid nitrogen vaporization rate. *J. Loss Prev. Process Ind.* **2013**, *26*, 398–409. [CrossRef]

12. Jiang, Z.; Huang, X.; Wu, Q.; Li, M.; Xie, Q.; Liu, Z.; Zou, X. Adsorption of sulfonamides on polyamide microplastics in an aqueous solution: Behavior, structural effects, and its mechanism. *Chem. Eng. J.* **2023**, *454*, 140452. [CrossRef]

13. Valluri, P.; Matar, O.K.; Mendes, M.; Hewitt, G.F. Modelling hydrodynamics and mass transfer in structured packings-a review. *Multiph. Sci. Technol.* **2002**, *14*, 46. [CrossRef]

14. Wood, D.A.; Choubineh, A.; Vaferi, B. Transparent open-box learning network provides auditable predictions: Pool boiling heat transfer coefficient for alumina-water-based nanofluids. *J. Therm. Anal. Calorim.* **2019**, *136*, 1395–1414. [CrossRef]

15. Keepaiboon, C.; Dalkilic, A.S.; Mahian, O.; Ahn, H.S.; Wongwises, S.; Mondal, P.K.; Shadloo, M.S. Two-phase flow boiling in a microfluidic channel at high mass flux. *Phys. Fluids* **2020**, *32*, 093309. [CrossRef]

16. Zhang, H.; Wang, H.; Niu, B.; Zhang, L.; Ahmad, A.M. Sliding-mode surface-based adaptive actor-critic optimal control for switched nonlinear systems with average dwell time. *Inf. Sci.* **2021**, *580*, 756–774. [CrossRef]

17. Liu, Y.; Olewski, T.; Véchot, L.N. Modeling of a cryogenic liquid pool boiling by CFD simulation. *J. Loss Prev. Process Ind.* **2015**, *35*, 125–134. [CrossRef]

18. Klimenko, V.; Sudarchikov, A. Investigation of forced flow boiling of nitrogen in a long vertical tube. *Cryogenics* **1983**, *23*, 379–385. [CrossRef]

19. Ishimoto, J.; Onishi, M.; Kamijo, K. Numerical and experimental study on the cavitating flow characteristics of pressurized liquid nitrogen in a horizontal rectangular nozzle. *J. Press. Vessel. Technol.* **2005**, *127*, 515–524. [CrossRef]

20. Li, X.; Wang, R.; Huang, R.; Shi, Y. Numerical investigation of boiling flow of nitrogen in a vertical tube using the two-fluid model. *Appl. Therm. Eng.* **2006**, *26*, 2425–2432. [CrossRef]

21. Zhang, X.; Jia, L.; Peng, Q.; Dang, C. Experimental study of condensation heat transfer in a condenser with a liquid-vapor separator. *Appl. Therm. Eng.* **2019**, *152*, 196–203. [CrossRef]

22. Zhang, C.; Sousa, A.C.; Venart, J.E. The numerical and experimental study of a power plant condenser. *ASME J. Heat Transfer* **1993**, *115*, 435–445. [CrossRef]

23. Zhang, X.; Jia, L.; Dang, C.; Peng, Q. Visualization investigation on flowing condensation in horizontal small channels with liquid separator. *J. Therm. Sci.* **2018**, *27*, 48–54. [CrossRef]

24. Oh, K.; Lee, S.; Park, T.; Kim, Y. Multistage Gas and Liquid Phase Separation Condenser. U.S. Patent No. 6,769,269, 3 August 2004.

25. Won, S.-P. Performance analysis of integral receiver/dryer condenser for automobile. *Korean J. Air-Cond. Refrig. Eng.* **2007**, *19*, 245–252.

26. Cho, H.; Cho, K. Mass flow rate distribution and phase separation of R-22 in multi-microchannel tubes under adiabatic condition. *Microscale Thermophys. Eng.* **2004**, *8*, 129–139. [CrossRef]

27. Zou, Y.; Hrnjak, P.S. Experiment and visualization on R134a upward flow in the vertical header of microchannel heat exchanger and its effect on distribution. *Int. J. Heat Mass Transf.* **2013**, *62*, 124–134. [CrossRef]

28. Li, H.; Hrnjak, P. An experimentally validated model for microchannel heat exchanger incorporating lubricant effect. *Int. J. Refrig.* **2015**, *59*, 259–268. [CrossRef]

29. Tu, J.; Yeoh, G. On numerical modelling of low-pressure subcooled boiling flows. *Int. J. Heat Mass Transf.* **2002**, *45*, 1197–1209. [CrossRef]

30. Yeoh, G.; Tu, J. Two-fluid and population balance models for subcooled boiling flow. *Appl. Math. Model.* **2006**, *30*, 1370–1391. [CrossRef]

31. Zuber, N. Hydrodynamic Aspects of Boiling Heat Transfer. Ph.D. Thesis, University of California, Riverside, CA, USA, 1959.

32. Chen, Y.; Hua, N.; Deng, L. Performances of a split-type air conditioner employing a condenser with liquid–vapor separation baffles. *Int. J. Refrig.* **2012**, *35*, 278–289. [CrossRef]

33. Hua, N.; Chen, Y.; Chen, E.; Deng, L.; Zheng, W.; Yang, Z. Prediction and verification of the thermodynamic performance of vapor–liquid separation condenser. *Energy* **2013**, *58*, 384–397. [CrossRef]

34. Alobaid, F.; Almohammed, N.; Farid, M.M.; May, J.; Rößger, P.; Richter, A.; Epple, B. Progress in CFD simulations of fluidized beds for chemical and energy process engineering. *Prog. Energy Combust. Sci.* **2021**, *91*, 100930. [CrossRef]

35. Alobaid, F.; Baraki, N.; Epple, B. Investigation into improving the efficiency and accuracy of CFD/DEM simulations. *Particuology* **2014**, *16*, 41–53. [CrossRef]

36. Sun, W.; Liu, L.; Memon, A.G.; Zhou, X.; Zhao, H. Waveguide-Based Fluorescent Immunosensor for the Simultaneous Detection of Carbofuran and 3-Hydroxy-Carbofuran. *Biosensors* **2020**, *10*, 191. [CrossRef] [PubMed]

37. Dhir, V.K. Numerical simulations of pool-boiling heat transfer. *AIChE J.* **2001**, *47*, 813–834. [CrossRef]

38. Son, G.; Dhir, V.K. Numerical simulation of film boiling near critical pressures with a level set method. *ASME J. Heat Transfer* **1998**, *120*, 183–192. [CrossRef]

39. Banerjee, D.; Dhir, V. Study of subcooled film boiling on a horizontal disc: Part I—Analysis. *J. Heat Transf.* **2001**, *123*, 271–284. [CrossRef]

40. Panzarella, C.H.; Davis, S.H.; Bankoff, S.G. Nonlinear dynamics in horizontal film boiling. *J. Fluid Mech.* **2000**, *402*, 163–194. [CrossRef]

41. Juric, D.; Tryggvason, G. Computations of boiling flows. *Int. J. Multiph. Flow* **1998**, *24*, 387–410. [CrossRef]

42. Esmaeeli, A.; Tryggvason, G. Computations of film boiling. Part II: Multi-mode film boiling. *Int. J. Heat Mass Transf.* **2004**, *47*, 5463–5476. [CrossRef]

43. Esmaeeli, A.; Tryggvason, G. Computations of film boiling. Part I: Numerical method. *Int. J. Heat Mass Transf.* **2004**, *47*, 5451–5461. [CrossRef]
44. Welch, S.W.; Wilson, J. A volume of fluid based method for fluid flows with phase change. *J. Comput. Phys.* **2000**, *160*, 662–682. [CrossRef]
45. Welch, S.W.; Rachidi, T. Numerical computation of film boiling including conjugate heat transfer. *Numer. Heat Transf. Part B Fundam.* **2002**, *42*, 35–53. [CrossRef]
46. Yuan, M.; Yang, Y.; Li, T.; Hu, Z. Numerical simulation of film boiling on a sphere with a volume of fluid interface tracking method. *Int. J. Heat Mass Transf.* **2008**, *51*, 1646–1657. [CrossRef]
47. Agarwal, D.; Welch, S.; Biswas, G.; Durst, F. Planar simulation of bubble growth in film boiling in near-critical water using a variant of the VOF method. *J. Heat Transf.* **2004**, *126*, 329–338. [CrossRef]
48. Tomar, G.; Biswas, G.; Sharma, A.; Welch, S. Multimode analysis of bubble growth in saturated film boiling. *Phys. Fluids* **2008**, *20*, 092101. [CrossRef]
49. Tomar, G.; Biswas, G.; Sharma, A.; Agrawal, A. Numerical simulation of bubble growth in film boiling using a coupled level-set and volume-of-fluid method. *Phys. Fluids* **2005**, *17*, 112103. [CrossRef]
50. Hens, A.; Biswas, G.; De, S. Analysis of interfacial instability and multimode bubble formation in saturated boiling using coupled level set and volume-of-fluid approach. *Phys. Fluids* **2014**, *26*, 012105. [CrossRef]
51. Welch, S.W.; Biswas, G. Direct simulation of film boiling including electrohydrodynamic forces. *Phys. Fluids* **2007**, *19*, 012106. [CrossRef]
52. Tomar, G.; Gerlach, D.; Biswas, G.; Alleborn, N.; Sharma, A.; Durst, F.; Welch, S.W.; Delgado, A. Two-phase electrohydrodynamic simulations using a volume-of-fluid approach. *J. Comput. Phys.* **2007**, *227*, 1267–1285. [CrossRef]
53. Amini, Y.; Karimi-Sabet, J.; Esfahany, M.N. Experimental and numerical study of multiphase flow in new wire gauze with high capacity structured packing. *Chem. Eng. Process. Process Intensif.* **2016**, *108*, 35–43. [CrossRef]
54. Fatehi, R.; Shadloo, M.S.; Manzari, M.T. Numerical investigation of two-phase secondary Kelvin–Helmholtz instability. *Proc. Inst. Mech. Eng. Part C J. MMech. Eng. Sci.* **2014**, *228*, 1913–1924. [CrossRef]
55. Amini, Y.; Nasr Esfahany, M. CFD simulation of the structured packings: A review. *Sep. Sci. Technol.* **2019**, *54*, 2536–2554. [CrossRef]
56. Amini, Y.; Ghazanfari, V.; Heydari, M.; Shadman, M.M.; Khamseh, A.G.; Khani, M.H.; Hassanvand, A. Computational fluid dynamics simulation of two-phase flow patterns in a serpentine microfluidic device. *Sci. Rep.* **2023**, *13*, 9483. [CrossRef]
57. Amini, Y.; Shadman, M.M.; Ghazanfari, Y.; Hassanvand, A. Enhancement of immiscible fluid mixing using passive micromixers to increase the performance of liquid–liquid extraction. *Inter. J. Modern Phys. C.* **2023**, *2350149*, 1–20. [CrossRef]
58. Aghel, B.; Rahimi, M.; Almasi, S. Experimental study on heat transfer characteristics of a modified two-phase closed thermosyphon. *Therm. Sci.* **2017**, *21*, 2481–2489. [CrossRef]
59. Rahimi, M.; Aghel, B.; Alsairafi, A. Experimental and CFD studies on using coil wire insert in a proton exchange membrane fuel cell. *Chem. Eng. Process. Process Intensif.* **2010**, *49*, 689–696. [CrossRef]
60. Hashemipour, N.; Karimi-Sabet, J.; Motahari, K.; Monfared, S.M.; Moosavian, M.A. Experimental and simulation investigation on separation of binary hydrocarbon mixture by thermogravitational column. *J. Mol. Liq.* **2018**, *268*, 791–806. [CrossRef]
61. Gerdroodbary, M.B.; Jafaryar, M.; Sheikholeslami, M.; Amini, Y. The efficacy of magnetic force on thermal performance of ferrofluid in a screw tube. *Case Stud. Therm. Eng.* **2023**, *49*, 103187. [CrossRef]
62. Li, Y.; Li, W.; Wan, L.; Xi, Y.; Wang, N. Numerical simulation of boiling two-phase flow in the subchannel under static state and rolling motion. *Int. J. Heat Mass Transf.* **2020**, *163*, 120416. [CrossRef]
63. Matsson, J.E. *An Introduction to ANSYS Fluent 2022*; SDC Publications: Mission, KS, USA, 2022.